Estimation on Location, Velocity, and Acceleration With High Precision for Collision Avoidance

Po-Jen Tu and Jean-Fu Kiang, *Member, IEEE*

***Abstract*—An approach is proposed to estimate the location, velocity, and acceleration of a target vehicle to avoid a possible collision. Radial distance, velocity, and acceleration are extracted from the hybrid linear frequency modulation (LFM)/frequency-shift keying (FSK) echoed signals and then processed using the Kalman filter and the trilateration process. This approach proves to converge fast with good accuracy. Two other approaches, i.e., an extended Kalman filter (EKF) and a two-stage Kalman filter (TSKF), are used as benchmarks for comparison. Several scenarios of vehicle movement are also presented to demonstrate the effectiveness of this approach.**

***Index Terms*—Kalman filter, radar, trilateration.**

I. Introduction

OVER one million people die in car accidents every year in the world, and more than 50 million are injured. An autonomous cruise-control (ACC) scheme has been reported to help in avoiding rear-end collisions, and a lane-departure warning/lane-change-assistance scheme has significantly reduced the number of car accidents [1]. A study shows that, in 29% of the cases, the driver did not hit the brake before an accident, because they either were not aware of the danger or had insufficient time to react [2]. An extra 0.5 s of early warning can prevent 60% of rear-end collisions [2].

Multiple types of sensors have been used in the ACC scheme, including image sensors, lidars, and radars [3]–[5]. Today, car manufacturers and their suppliers are developing a long-range radar to cover a maximum range of 200 m within the azimuthal range of 14°. Short-range radars with coverage up to 30 m and an azimuthal range of 140° are also under development [6], [7].

Precise detection of a nearby moving target is critical for the ACC scheme to effectively work. Several methods have been proposed to trilaterate a specific target based on multiple radar sensors. In [8], Klotz presents a method to trilaterate a target using multiple frequency-modulated continuous-wave (FMCW) echoes. A linear Kalman filter can be used to estimate the relative range and velocity based on the range data recorded with a sensor [9]. However, the acceleration cannot reliably be estimated, for example, when the target is making a turn over a short period. Another two-stage linear Kalman filter (TSLKF) is capable of estimating the relative acceleration [10]. However, it slowly converges if the target is making a quick turn. An extended Kalman filter (EKF) has been used to estimate the kinematic parameters of the target using only one sensor [11]. However, the errors become too large when the target is making a turn.

In this paper, a robust Kalman filter (RKF) is proposed to improve the estimation accuracy of acceleration and, hence, that of location. The proposed approach is presented in Section II. The TSLKF and the EKF are briefly reviewed in Section III. In Section IV, the accuracy of these approaches is compared under several scenarios, with the target vehicle making a turn in front of the host vehicle.

Manuscript received July 28, 2007; revised April 8, 2008, February 26, 2009, September 22, 2009, and December 10, 2009; accepted February 3, 2010. Date of publication March 8, 2010; date of current version May 25, 2010. This work was supported by the National Science Council, Taiwan, under Contract NSC 93-2213-E-002-034. The Associate Editor for this paper was R. W. Goudy.

The authors are with the Department of Electrical Engineering and the Graduate Institute of Communication Engineering, National Taiwan University, Taipei 106, Taiwan (e-mail: r94942069@ntu.edu.tw; jfkiang@cc.ee.ntu.edu.tw).

Digital Object Identifier 10.1109/TITS.2010.2043098

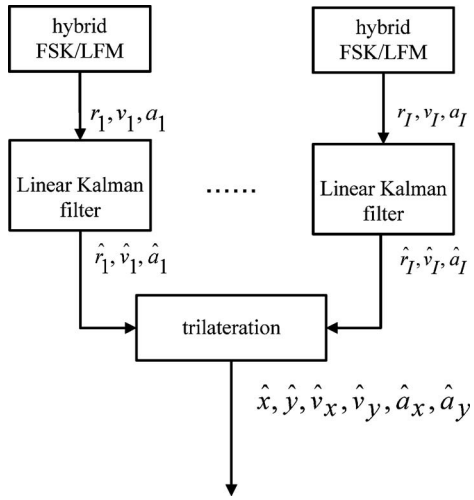

Fig. 1. Procedure of robust Kalman filter.

II. Robust Kalman Filter

Fig. 1 shows the RKF, which consists of three stages: First, data of range r_i, radial velocity v_i, and radial acceleration a_i are extracted from the echoed signals reflected by the target and received by the ith sensor. Second, a linear Kalman filter is used to estimate $\hat{r}_i(t)$, $\hat{v}_i(t)$, and $\hat{a}_i(t)$. Third, the trilateration process is applied to estimate the kinematic parameters of the target $\hat{x}(t)$, $\hat{y}(t)$, $\hat{v}_x(t)$, $\hat{v}_y(t)$, $\hat{a}_x(t)$, and $\hat{a}_y(t)$.

A. Hybrid FSK and LFM Signals

Fig. 2 shows the temporal variation of frequency of a linear frequency-modulation (LFM) signal [12], with bandwidth B_{sweep} and dwell time T_{LFM}. Fig. 3 shows a frequency-shift keying (FSK) scheme by using two LFM signals A and B with

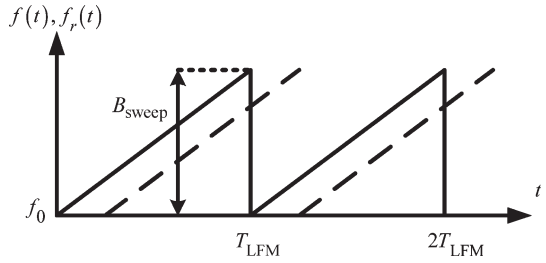

Fig. 2. Frequency variation of the LFM signal. (Solid line) $f(t)$ of the transmitted signal. (Dashed line) $f_r(t)$ of the received signal.

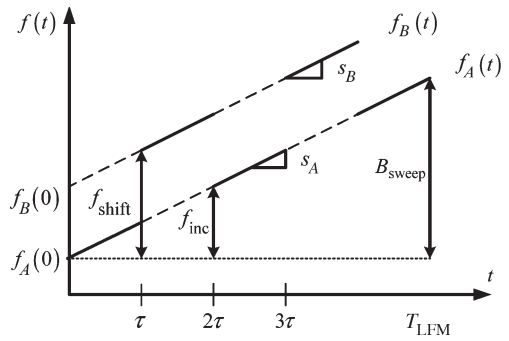

Fig. 3. Hybrid FSK and LFM signals.

frequency-changing rates of s_A and s_B, respectively. In this paper, we choose $s_A = s_B = s$ without loss of generality. By taking $2N$ samples with interval $\tau = T_{\text{LFM}}/2N$, the frequency increment over 2τ becomes $f_{\text{inc}} = B_{\text{sweep}}/N$. A typical set of parameters, e.g., are $f_A(0) = 77$ GHz, $B_{\text{sweep}} = 150$ MHz, $f_B(t) - f_A(t) = 300$ kHz, $T_{\text{LFM}} = 51.2$ ms, and $N = 256$ [12]. The frequency difference between the second signal measured at $t = 2n\tau$ and the first signal at $t = (2n-1)\tau$ is $f_{\text{shift}} = f_B(0) - f_A(0) + s\tau$.

The frequency differences between the echoed signals and the emitted signals are $\Delta f_A = f_{rA}(t) - f_A(t)$ and $\Delta f_B = f_{rB}(t) - f_B(t)$. Define $S_A = \Delta f_A T_{\text{LFM}}$ and $S_B = \Delta f_B T_{\text{LFM}}$; then

$$\begin{aligned} S_A &= T_{\text{LFM}}\left[f_{rA}(t) - f_A(t)\right] \\ &= T_{\text{LFM}}\left\{\left[f_0 + s(t - 2r_A/c)\right](1 - 2v_A/c) - (f_0 + st)\right\} \\ &= T_{\text{LFM}}\left[-(2v_A/c)f_A(t) - (2sr_A/c)(1 - 2v_A/c)\right] \\ &\simeq T_{\text{LFM}}\left[-(2s/c)r_A - (2v_A/c)f_A(t)\right] \qquad (1) \\ S_B &= T_{\text{LFM}}\left[f_{rB}(t) - f_B(t)\right] \\ &\simeq T_{\text{LFM}}\left[-2sr_B/c - (2v_B/c)f_B(t)\right] \\ &= T_{\text{LFM}}\big[-(2s/c)(r_A + v_A\tau + a\tau^2/2) \\ &\qquad - (2/c)(v_A + a\tau)f_B(t)\big] \\ &= T_{\text{LFM}}\left\{-(2s/c)r_A - (2/c)\left[f_B(t) + s\tau\right]v_A\right. \\ &\qquad \left. - (2/c)\left[\tau f_B(t) + s\tau^2/2\right]a\right\} \qquad (2) \end{aligned}$$

during $0 < t < T_{\text{LFM}}$, where r_A and v_A are the range and velocity, respectively, measured at $t = (2n-1)\tau$; and r_B and v_B are the range and velocity, respectively, measured at $t = 2n\tau$. The acceleration a is approximated as a constant during $0 < t < T_{\text{LFM}}$. The phase difference between the second signal measured at $t = 2n\tau$ and the first signal measured at $t = (2n-1)\tau$ is

$$\begin{aligned} \Delta\varphi &= \varphi_B - \varphi_A \\ &= \frac{4\pi}{c}\left\{\left[f_B(0) + 2ns\tau - \frac{2sr_B}{c}\right]\left(1 - \frac{2v_B}{c}\right)r_B\right. \\ &\qquad - \left[f_A(0) + (2n-1)s\tau - \frac{2sr_A}{c}\right] \\ &\qquad \left.\times\left(1 - \frac{2v_A}{c}\right)r_A\right\} \\ &\simeq \frac{4\pi}{c}\left\{\left[f_B(0) + 2ns\tau - \frac{2sr_B}{c}\right]r_B\right. \\ &\qquad \left. - \left[f_A(0) + (2n-1)s\tau - \frac{2sr_A}{c}\right]r_A\right\} \\ &\simeq \frac{4\pi}{c}f_{\text{shift}}r_A + \frac{4\pi}{c}f_B(t)\left(v_A\tau + \frac{1}{2}a\tau^2\right). \qquad (3) \end{aligned}$$

Equations (1)–(3) can be reorganized as

$$\begin{bmatrix} r \\ v \\ a \end{bmatrix} = \begin{bmatrix} r_A \\ v_A \\ a \end{bmatrix} = \bar{\bar{J}}^{-1} \cdot \begin{bmatrix} -S_A c/T_{\text{LFM}} \\ -S_B c/T_{\text{LFM}} \\ \Delta\varphi c/\pi \end{bmatrix}$$

where

$$\bar{\bar{J}} = \begin{bmatrix} 2s & 2f_A(t) & 0 \\ 2s & 2\left[f_B(t) + s\tau\right] & 2\left[f_B(t)\tau + s\tau^2/2\right] \\ 4f_{\text{shift}} & 4f_B(t)\tau & 2f_B(t)\tau^2 \end{bmatrix}.$$

Reasonable accuracy of range and velocity estimation can be achieved by choosing $f_{\text{shift}} = -f_{\text{inc}}/2$ [12].

B. Kalman Filter

The Kalman filter in [13] is summarized as

$$\begin{aligned} \bar{\bar{R}}_\alpha[n] &= \bar{\bar{C}}[n] \cdot \bar{\bar{K}}[n|n-1] \cdot \bar{\bar{C}}^\dagger[n] + \bar{\bar{Q}}_2 \\ \bar{\bar{G}}[n] &= \bar{\bar{K}}[n|n-1] \cdot \bar{\bar{C}}^\dagger[n] \cdot \bar{\bar{R}}_\alpha^{-1}[n] \\ \bar{\alpha}[n] &= \bar{y}[n] - \bar{\bar{C}}[n] \cdot \hat{x}[n|n-1] \\ \hat{x}[n|n] &= \hat{x}[n|n-1] + \bar{\bar{G}}[n] \cdot \bar{\alpha}[n] \\ \hat{x}[n+1|n] &= \bar{\bar{F}}[n+1|n] \cdot \hat{x}[n|n] \\ \bar{\bar{K}}_\varepsilon[n] &= \bar{\bar{K}}[n|n-1] - \bar{\bar{G}}[n] \cdot \bar{\bar{C}}[n] \cdot \bar{\bar{K}}[n|n-1] \\ \bar{K}[n+1|n] &= \bar{\bar{F}}[n+1|n] \cdot \bar{\bar{K}}_\varepsilon[n] \cdot \bar{\bar{F}}^\dagger[n+1|n] + \bar{\bar{Q}}_1 \end{aligned}$$

where $\bar{\alpha}[n]$ is the innovation vector, $\hat{x}[n|n]$ is the filtered estimate of the state vector, $\hat{x}[n+1|n]$ is the predicted estimate of the state vector, $\bar{y}[n]$ is the measurement vector, $\bar{\bar{R}}_\alpha[n]$ is the correlation matrix of $\bar{\alpha}[n]$, $\bar{\bar{G}}[n]$ is the Kalman gain, $\bar{\bar{K}}_\varepsilon[n]$ is the correlation matrix of $\hat{x}[n|n]$, $\bar{\bar{K}}[n+1|n]$ is the correlation matrix of $\hat{x}[n+1|n]$, $\bar{\bar{C}}[n]$ is the measurement matrix, $\bar{\bar{F}}[n+1|n]$ is the transition matrix, and $\bar{\bar{Q}}_1$ and $\bar{\bar{Q}}_2$ are the correlation

matrices of the process noise vector and the measurement noise vector, respectively.

The measurement vector $\bar{y}_j[n]$ and the dynamic state vector $\bar{x}_j[n]$ associated with the jth sensor are defined as

$$\bar{y}_j[n] = \begin{bmatrix} r_j[n] \\ v_j[n] \\ a_j[n] \end{bmatrix} \qquad \bar{x}_j[n] = \begin{bmatrix} \hat{r}_j[n] \\ \hat{v}_j[n] \\ \hat{a}_j[n] \end{bmatrix}$$

with $j = 1, 2$. The state transition matrix can be derived as

$$\bar{\bar{F}}[n+1|n] = \begin{bmatrix} 1 & T_p & T_p^2/2 \\ 0 & 1 & T_p \\ 0 & 0 & 1 \end{bmatrix}$$

where $T_p = 2\tau$ is the time interval for state update. Assume $\bar{\bar{C}}[n] = \bar{\bar{I}}_{3\times 3}$, $\bar{\bar{Q}}_1 = \bar{\bar{0}}$, and

$$\bar{\bar{Q}}_2 = \begin{bmatrix} \sigma_r^2 & 0 & 0 \\ 0 & \sigma_v^2 & 0 \\ 0 & 0 & \sigma_a^2 \end{bmatrix}.$$

The initial values are chosen as $\bar{x}_j[1|0] = [r_j[0] v_j[0] a_j[0]]^t$ and $\bar{\bar{K}}[1|0] = \bar{\bar{I}}_{3\times 3}$.

With reference to [14], the standard deviations of range and velocity measurement are chosen as $\sigma_r = 0.05$ m and $\sigma_v = 0.02$ m/s, respectively. The standard deviation of acceleration is chosen as $\sigma_a = 1$ m/s^2. The data received by each sensor are independently processed.

C. Trilateration

Without loss of generality, assume that the ith sensor is located at $(x_i, 0)$, and the reflecting point of the target vehicle is located at $(\hat{x}, \hat{y})$, moving at velocity $(\hat{v}_x, \hat{v}_y)$. The output from the Kalman filter based on the data received at the ith sensor is $\hat{r}_i$, $\hat{v}_i$, and $\hat{a}_i$. The ranges $\hat{r}_1$ and $\hat{r}_2$ can be expressed as

$$\hat{r}_1^2 = (\hat{x} - x_1)^2 + \hat{y}^2$$
$$\hat{r}_2^2 = (\hat{x} - x_2)^2 + \hat{y}^2.$$

By eliminating $\hat{y}$, we have

$$\hat{x} = \frac{x_1^2 - x_2^2 - \hat{r}_1^2 + \hat{r}_2^2}{2(x_1 - x_2)}. \tag{4}$$

Then, $\hat{y}$ can be determined as

$$\hat{y} = \sqrt{\hat{r}_1^2 + \hat{r}_2^2 - (\hat{x} - x_1)^2 - (\hat{x} - x_2)^2} \Big/ \sqrt{2}. \tag{5}$$

The relative velocities $\hat{v}_1$ and $\hat{v}_2$ are related to $\hat{v}_x$ and $\hat{v}_y$ as

$$\hat{v}_1 = \frac{\hat{x} - x_1}{\hat{r}_1}\hat{v}_x + \frac{\hat{y}}{\hat{r}_1}\hat{v}_y$$
$$\hat{v}_2 = \frac{\hat{x} - x_2}{\hat{r}_2}\hat{v}_x + \frac{\hat{y}}{\hat{r}_2}\hat{v}_y.$$

The target velocity can thus be derived as

$$\begin{bmatrix} \hat{v}_x \\ \hat{v}_y \end{bmatrix} = \begin{bmatrix} \hat{x} - x_1 & \hat{y} \\ \hat{x} - x_2 & \hat{y} \end{bmatrix}^{-1} \begin{bmatrix} \hat{v}_1 \hat{r}_1 \\ \hat{v}_2 \hat{r}_2 \end{bmatrix}. \tag{6}$$

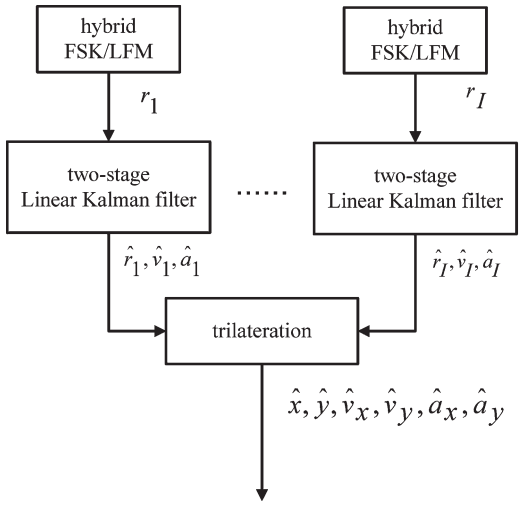

Fig. 4. Procedure of the TSLKF.

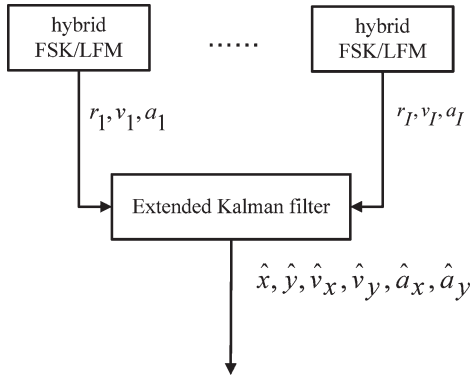

Fig. 5. Procedure of the EKF.

Similarly, the target accelerations $\hat{a}_x$ and $\hat{a}_y$ can be derived from the relative accelerations $\hat{a}_1$ and $\hat{a}_2$ as

$$\begin{bmatrix} \hat{a}_x \\ \hat{a}_y \end{bmatrix} = \begin{bmatrix} \hat{x} - x_1 & \hat{y} \\ \hat{x} - x_2 & \hat{y} \end{bmatrix}^{-1} \begin{bmatrix} \hat{a}_1 \hat{r}_1 \\ \hat{a}_2 \hat{r}_2 \end{bmatrix}. \tag{7}$$

III. Other Kalman Filters for Comparison

A. TSLKF

Fig. 4 shows the procedure of the TSLKF [10]. Its estimation is based on a linear combination of the outputs from a bias-free filter and a biased filter. The output of the biased filter is used to correct that of the bias-free filter in estimating the target range and velocity. First, ranges r_i from the target to the sensors are extracted from the LFM echoed signals [15]; then, these r_i's are sent to the two-stage Kalman filter to estimate $\hat{r}_i(t)$, $\hat{v}_i(t)$, and $\hat{a}_i(t)$ [16]. Second, the trilteration equations in (4)–(7) are used to estimate $\hat{x}(t)$, $\hat{y}(t)$, $\hat{v}_x(t)$, $\hat{v}_y(t)$, $\hat{a}_x(t)$, and $\hat{a}_y(t)$.

B. EKF

Fig. 5 shows the procedure of the EKF [17]. Taylor approximation is applied to linearize the transition and measurement matrices, which are originally nonlinear. First, ranges r_i, velocities v_i, and accelerations a_i from the target to the sensors are

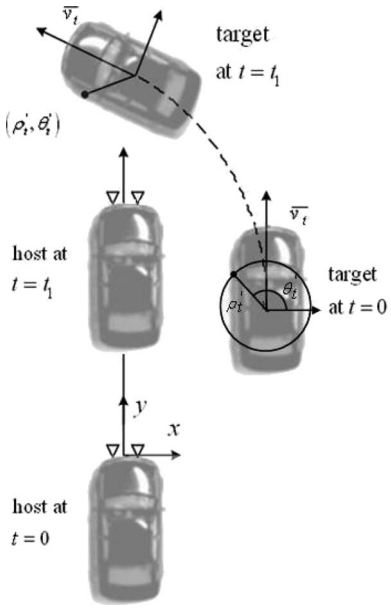

Fig. 6. Target vehicle makes a left turn in front of the host vehicle. (Solid line) Host trajectory. (Dashed line) Target trajectory.

extracted from the hybrid FSK/LFM echoed signals received at the sensors. These data are then sent to the EKF to estimate $\hat{x}(t)$, $\hat{y}(t)$, $\hat{v}_x(t)$, $\hat{v}_y(t)$, $\hat{a}_x(t)$, and $\hat{a}_y(t)$.

IV. Results and Discussions

Fig. 6 shows a typically dangerous scenario when a target vehicle tries to make a left turn across the lane of the host vehicle. Let both vehicles be driven on the xy-plane, and the center of the front bumper on the host vehicle is chosen as a reference point. Assume that there are two sensors installed on the front bumper of the host vehicle, i.e., one is 0.8 m to the left, and the other is 0.8 m to the right of the reference point. The host vehicle moves straight ahead in the $\hat{y}$ direction at a constant speed.

Assume that the target vehicle is in the right front of the host vehicle at $t = 0$ and then starts to make a left turn at the speed of v_{Rt} and with the radius of curvature R_t, creating a centrifugal acceleration of $a_{Rt} = v_{Rt}^2/R_t$.

As shown in Fig. 6, the center of mass of the target vehicle is at $(x_t(t), y_t(t))$, and the local polar coordinates of a point on the target vehicle are (ρ'_t, θ'_t). Hence, the trajectory of the given point on the target vehicle can be expressed as

$$x'_t(t) = x_t(t) + \rho'_t \cos\theta'_t(t)$$
$$y'_t(t) = y_t(t) + \rho'_t \sin\theta'_t(t)$$

where

$$\theta'_t(t) = \tan^{-1}\left[\frac{v_{ty}(t)}{v_{tx}(t)}\right] + \phi'_t - 90^\circ.$$

ρ'_t is the radius from the center of the mass, θ'_t is the polar angle of the given point in the local coordinate, and ϕ'_t is the initial azimuthal angle of the local coordinate with respect to the reference coordinate.

The relative position, velocity, and acceleration of the given point $(x'_t, y'_t, v'_{tx}, v'_{ty}, a'_{tx}, a'_{ty})$, with respect to those of the reference point $(x'_h, y'_h, v'_{hx}, v'_{hy}, a'_{hx}, a'_{hy})$, are

$$x'(t) = x'_t(t) - x_h(t), \qquad y'(t) = y'_t(t) - y_h(t)$$
$$v'_x(t) = v'_{tx}(t) - v_{hx}(t), \qquad v'_y(t) = v'_{ty}(t) - v_{hy}(t)$$
$$a'_x(t) = a'_{tx}(t) - a_{hx}(t), \qquad a'_y(t) = a'_{ty}(t) - a_{hy}(t).$$

The radial distance, velocity, and acceleration between the target and the ith sensor can thus be expressed as [17]

$$r_i(t) = \sqrt{[x'(t) - x_i]^2 + [y'(t) - y_i]^2}$$
$$v_i(t) = \frac{x'(t) - x_i}{r_i(t)} v'_x(t) + \frac{y'(t) - y_i}{r_i(t)} v'_y(t)$$
$$a_i(t) = \frac{x'(t) - x_i}{r_i(t)} a'_x(t) + \frac{y'(t) - y_i}{r_i(t)} a'_y(t).$$

The length and width of both vehicles are chosen as 4 and 1.8 m, respectively. The initial kinematic parameters of the host vehicle are $x_h(0) = 0$, $y_h(0) = 0$, $v_{hx}(0) = 0$, $v_{hy}(0) = 20$ m/s, $a_{hx}(0) = 0$, and $a_{hy}(0) = 0$. The initial kinematic parameters of the target vehicle are $x_t(0) = 8$ m, $y_t(0) = 11$ m, $v_{tx}(0) = 0$, and $v_{ty}(0) = 12$ m/s. At $t = 0$, the target vehicle begins to make a circular motion with the speed of $v_{Rt} = 12$ m/s (43.2 km/h) and the radius of $R_t = 15$ m, rendering an acceleration of magnitude $|a_{Rt}| = 14.4$ m/s^2, which implies $a_{tx}(0) = -14.4$ m/s^2, and $a_{ty}(0) = 0$.

Monte Carlo simulation is applied with $M = 100$ trials. Fig. 7 shows the time evolution of estimation errors using the proposed RKF, TSLKF, and EKF approaches. The medium cases in terms of acceleration error among the 100 trials in each approach are presented.

The RMS errors of estimated kinematic parameters at $t = 1800T_p$ using RKF are $\varepsilon_x = 0.0049$ m, $\varepsilon_y = 0.0088$ m, $\varepsilon_{v_x} = 0.83$ m/s, $\varepsilon_{v_y} = 0.92$ m/s, $\varepsilon_{a_x} = 6.1$ m/s^2, and $\varepsilon_{a_y} = 0.92$ m/s^2. The RMS errors are defined as

$$\varepsilon_\alpha = \sqrt{\frac{1}{M}\sum_{n=1}^{M}\left[\hat{\alpha}^{(n)} - \alpha\right]^2}$$

where $\alpha = x, y, v_x, v_y, a_x$, and a_y, and the superscript (n) indicates the nth trial of the Monte Carlo simulation.

The RMS errors using TSLKF are $\varepsilon_x = 0.023$ m, $\varepsilon_y = 0.035$ m, $\varepsilon_{v_x} = 0.38$ m/s, $\varepsilon_{v_y} = 0.84$ m/s, $\varepsilon_{a_x} = 7.5$ m/s^2, and $\varepsilon_{a_y} = 4.9$ m/s^2. The RMS errors using EKF are $\varepsilon_x = 3.2$ m, $\varepsilon_y = 2.8$ m, $\varepsilon_{v_x} = 0.028$ m/s, $\varepsilon_{v_y} = 6.5$ m/s, $\varepsilon_{a_x} = 5.3$ m/s^2, and $\varepsilon_{a_y} = 12.8$ m/s^2. It is observed that the errors in a_x and a_y using both TSLKF and EKF are larger than those using RKF.

Fig. 8 shows the cumulative distribution of errors in estimating the acceleration at $t = 1800T_p$ over those 100 trials. The errors of RKF are smaller than those of TSLKF and EKF. The errors of EKF spread over a wide range, whereas those of RKF and TSLKF appear to be almost constant.

To compare the performance of these three approaches over a wider range of kinematic parameters, we demonstrate another four scenarios of the target vehicle making a left turn in front

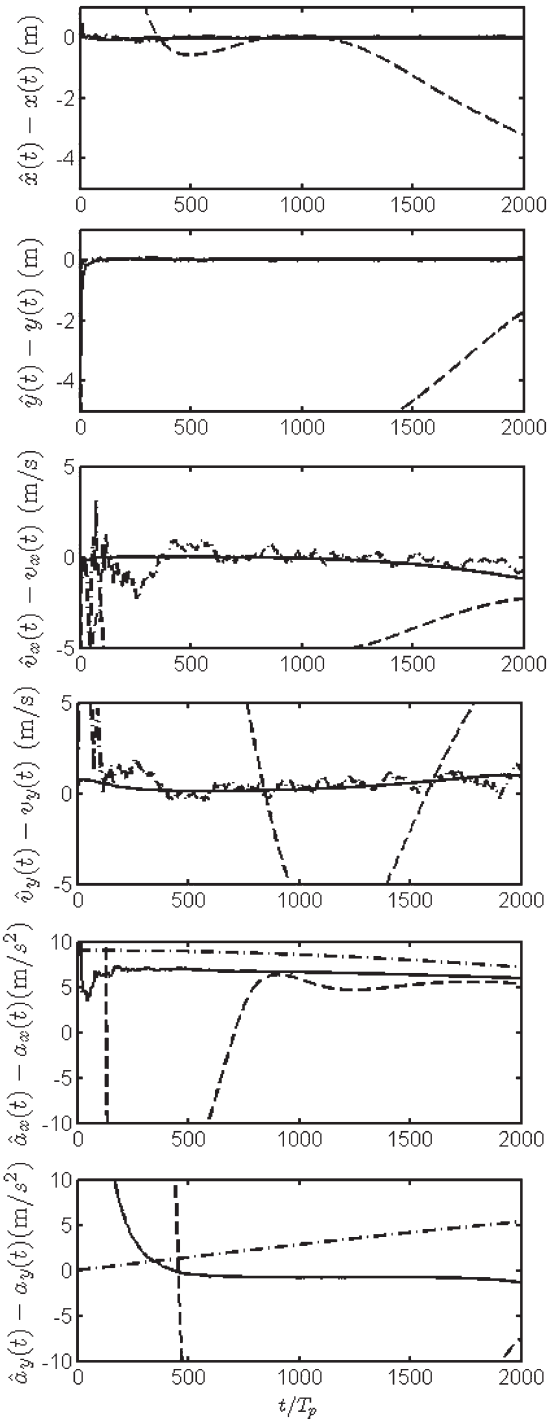

Fig. 7. Estimation errors. (Solid line) RKF with $T_p = 200$ μs, $\sigma_r = 0.05$ m, $\sigma_v = 0.02$ m/s, and $\sigma_a = 1$ m/s^2. (Dash-dotted line) TSLKF with $T_p = 200$ μs, $\sigma_r = 0.05$ m, $\sigma_v = 0.02$ m/s, and $\mathrm{E}\{a^2\} = 400$ m^2/s^4 [10]. (Dashed line) EKF with $T_p = 200$ μs, $\sigma_r = 0.05$ m, $\sigma_v = 0.02$ m/s, and $\sigma_a = 1$ m/s^2 [18].

of the host vehicle at different speeds and different radii of curvature. Table I lists the RMS errors using Monte Carlo simulation with $M = 100$ trials. Table II lists the errors of predicted coordinates at the critical time t_c using the medium case of each approach.

In scenarios 1 and 3, the target vehicle is expected to impact the host vehicle at the critical time. In scenarios 2 and 4, the two vehicles will not collide, because the target vehicle moves either too fast or too slowly.

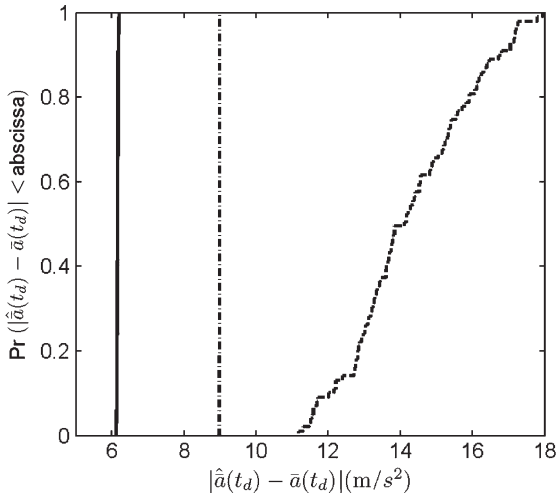

Fig. 8. Cumulative distribution of errors in estimating acceleration at $t = t_d = 1800T_p$. (Solid line) RKF. (Dash-dotted line) TSLKF. (Dashed line) EKF. The parameters are the same as those in Fig. 7.

TABLE I
RMS ERRORS OF ESTIMATED KINEMATIC PARAMETERS

	ε_x(m)	ε_y(m)	ε_{v_x}(m/s)	ε_{v_y}(m/s)	ε_{a_x}(m/s^2)	ε_{a_y}(m/s^2)
RKF(S1)	0.037	0.0124	2.69	1.26	3.12	1.32
TSLKF(S1)	0.029	0.114	1.07	2.25	7.14	10.84
EKF(S1)	0.075	0.266	0.69	0.41	3.46	4.71
RKF(S2)	0.023	0.03	0.15	0.25	15.14	31.86
TSLKF(S2)	0.063	0.023	5.58	1.92	58.61	59.24
EKF(S2)	4.72	11.82	12.06	0.28	6.42	84.71
RKF(S3)	0.009	0.004	1.63	0.87	4.17	7.02
TSLKF(S3)	0.037	0.018	1.71	0.2	15.51	10.88
EKF(S3)	5.16	7.48	3.6	10.83	9.66	50.27
RKF(S4)	0.017	0.012	0.018	0.071	0.228	0.445
TSLKF(S4)	0.048	0.034	0.57	0.59	1.59	7.81
EKF(S4)	6.16	5.04	3.77	10.53	26.38	51.79

S1(Scenario 1): $v_y = 12$ m/s, $R_t = 10$ m ($t_c = 0.8$ s)
S2(Scenario 2): $v_y = 30$ m/s, $R_t = 10$ m ($t_c = 0.4$ s)
S3(Scenario 3): $v_y = 20$ m/s, $R_t = 15$ m ($t_c = 0.6$ s)
S4(Scenario 4): $v_y = 8$ m/s, $R_t = 20$ m ($t_c = 0.4$ s)

TABLE II
RMS ERRORS OF PREDICTED COORDINATES AT CRITICAL TIME

	RKF (x, y) (m)	TSLKF (x, y) (m)	EKF (x, y) (m)	critical time (s)
S1	$(0.037, 0.012)$	$(0.029, 0.11)$	$(0.075, 0.27)$	0.8
S2	$(0.023, 0.03)$	$(0.063, 0.023)$	$(4.7, 11.8)$	0.4
S3	$(0.009, 0.004)$	$(0.037, 0.018)$	$(5.2, 7.5)$	0.6
S4	$(0.017, 0.012)$	$(0.048, 0.034)$	$(6.2, 5.0)$	0.4

S1, S2, S3, S4 are the same as in Table I.

Scenario 1: The target vehicle makes a left turn at the speed of $v_{Rt} = 12$ m/s (43.2 km/h) with a radius of curvature $R_t = 10$ m. Thus, the initial values are $v_{ty}(0) = 12$ m/s and $a_{tx}(0) = -14.4$ m/s^2. The RMS errors of kinematic parameters at $t = 0.8$ s are listed in the three rows marked by S1 in Table I. The errors in a_x and a_y using both TSLKF and EKF are larger than those using RKF.

Scenario 2: The target vehicle makes a left turn at the speed of $v_{Rt} = 30$ m/s (108 km/h) with a radius of curvature

$R_t = 10$ m. Thus, the initial values are $v_{ty}(0) = 30$ m/s and $a_{tx}(0) = -90$ m/s^2. The RMS errors of kinematic parameters at $t = 0.4$ s are listed in the three rows marked by S2 in Table I. The EKF cannot keep track of the target. The RMS errors using TSLKF and EKF are larger than those using RKF.

Scenario 3: The target vehicle makes a left turn at the speed of $v_{Rt} = 20$ m/s (72 km/h) with a radius of curvature $R_t = 15$ m. Thus, the initial values are $v_{ty}(0) = 20$ m/s and $a_{tx}(0) = -26.67$ m/s^2. The RMS errors of kinematic parameters at $t = 0.6$ s are listed in the three rows marked by S3 in Table I. The EKF loses track of the target again.

Scenario 4: The target vehicle makes a left turn at the speed of $v_{Rt} = 8$ m/s (28.8 km/h) with a radius of curvature $R_t = 20$ m. Thus, the initial values are $v_{ty}(0) = 8$ m/s and $a_{tx}(0) = -3.2$ m/s^2. The RMS errors of kinematic parameters at $t = 0.4$ s are listed in the three rows marked by S4 in Table I. The EKF fails again.

These four scenarios give a general comparison of the three approaches under different conditions of vehicle movement. In scenarios 1 and 3, the target vehicle turns at a normal speed with a normal radius. The proposed RKF delivers better estimations than the other two approaches. In scenario 2, the target vehicle makes a faster turn with a smaller radius. The EKF cannot quickly converge, and the TSLKF delivers poor estimation of acceleration. In scenario 4, the target vehicle makes a slower turn with a larger radius, and the RKF also delivers the least estimation errors among the three approaches.

The EKF fails to track the target due to its nonlinear transformation from the radial kinematic parameters to those in the Cartesian coordinates without trilateration. The RKF consistently renders smaller errors in the estimation of position, velocity, and acceleration than the other two approaches. The TSLKF uses only the radial distances as the input to the Kalman filter, which are fewer than those in the RKF; hence, the estimation errors using the former are expected to be larger than those using the latter. The proposed RKF more accurately predicts the target vehicle position at the critical time than the other two approaches.

V. Conclusion

An RKF is proposed to estimate the location, velocity, and acceleration of a target vehicle with a fast convergence rate and high accuracy. Data of radial distance, velocity, and acceleration are extracted from the echoed LFM/FSK signals. TSLKF and EKF are also used to compare the performance of this approach. Several scenarios with a vehicle making a left turn in front of the host vehicle are used to demonstrate the effectiveness of this approach.

References

[1] The Commissions Intelligent Car Flagship Under the i2010 Initiative, Brussels, Feb. 21, 2006. [Online]. Available: http://europa.eu/rapid/pressReleasesAction.do?reference=MEMO/06/86

[2] Accident Prevention and Accident Mitigation, Mobileye, Amstelveen, The Netherlands. [Online]. Available: http://www.mobileye-vision.com/Publications/AWS.EffectivenessReport.pdf

[3] H. Cheng, N. Zheng, X. Zhang, J. Qin, and H. van de Wetering, "Interactive road situation analysis for driver assistance and safety warning systems: Framework and algorithm," *IEEE Trans. Intell. Transp. Syst.*, vol. 8, no. 1, pp. 157–167, Mar. 2007.

[4] S. Pietzsch, T. D. Vu, J. Burlet, O. Aycard, T. Hackbarth, N. Appenrodt, J. Dickmann, and B. Radig, "Results of a precrash application based on laser scanner and short-range radars," *IEEE Trans. Intell. Transp. Syst.*, vol. 10, no. 4, pp. 584–593, Dec. 2009.

[5] S. G. Wu, S. Decker, P. Chang, T. Camus, and J. Eledath, "Collision sensing by stereo vision and radar sensor fusion," *IEEE Trans. Intell. Transp. Syst.*, vol. 10, no. 4, pp. 606–614, Dec. 2009.

[6] F. Florian and H. Rohling, "Signal processing structure for automotive radar," *Frequenz*, no. 1/2, pp. 20–23, Jan./Feb. 2006.

[7] J. Wenger, "Automotive radar—Status and perspectives," in *Proc. IEEE Compound Semicond. Integr. Circuit Symp.*, Oct. 2005, pp. 21–24.

[8] M. Klotz, "An automotive short range high resolution pulse radar network," Ph.D. dissertation, Technische Univ. Hamburg-Harburg, Hamburg, Germany, 2002.

[9] P. Mookerjee and F. Reifler, "Reduced state estimators for consistent tracking of maneuvering targets," *IEEE Trans. Aerosp. Electron. Syst.*, vol. 41, no. 2, pp. 608–619, Apr. 2005.

[10] C. S. Heish and F. C. Chen, "General two-stage Kalman filters," *IEEE Trans. Autom. Control*, vol. 45, no. 4, pp. 819–824, Apr. 2000.

[11] P. Gurfil, "Two-step optimal estimator for three dimensional target tracking," *IEEE Trans. Aerosp. Electron. Syst.*, vol. 41, no. 3, pp. 780–793, Jul. 2005.

[12] H. Rohling and M. M. Meinecke, "Waveform design principles for automotive radar systems," in *Proc. IEEE Radar*, Oct. 2001, pp. 1–4.

[13] S. Haykin, *Adaptive Filter Theory*., 4th ed. Englewood Cliffs, NJ: Prentice-Hall, 2002.

[14] J. V. Kleff, J. Bergmans, and L. Kester, Multiple-hypothesis trilateration and tracking with distributed radars. [Online]. Available: http://staff.science.uva.nl/~jvanklee/Publications/data/174.pdf .

[15] D. C. Schleher, *MTI and Pulse Doppler Radar*. Norwood, MA: Artech House, 1991.

[16] M. B. Ignagni, "An alternate derivation and extension of Friendlands two-stage Kalman estimator," *IEEE Trans. Autom. Control*, vol. AC-26, no. 3, pp. 746–750, Jun. 1981.

[17] Y. N. Chung, D. L. Gustafson, and E. Emer, "Extended solution to multiple maneuvering target tracking," *IEEE Trans. Aerosp. Electron. Syst.*, vol. 26, no. 5, pp. 876–887, Sep. 1990.

[18] F. Folster, H. Rohling, and U. Lubbert, "An automotive radar network based on 77 GHz FMCW sensors," in *Proc. IEEE Int. Conf. Radar*, May 2005, pp. 871–876.

Po-Jen Tu was born in Keelung, Taiwan, on December 11, 1982. He received the B.S. degree in communications engineering from Yuan-Ze University, Taoyuan, Taiwan, in 2005 and the M.S. degree in communication engineering from National Taiwan University, Taipei, Taiwan, in 2007.

Jean-Fu Kiang (M'08) was born in Taipei, Taiwan, on February 2, 1957. He received the B.S. and M.S. degrees in electrical engineering from National Taiwan University, Taipei, in 1979 and 1981, respectively, and the Ph.D. degree in electrical engineering from the Massachusetts Institute of Technology, Cambridge, in 1989.

During the summers of 1985 and 1986, he was with Schlumberger-Doll Research, Ridgefield, CT. From 1989 to 1990, he was with the IBM T. J. Watson Research Center, Yorktown Heights, NY. From 1990 to 1992, he was with Bellcore, Red Bank, NJ. From 1992 to 1994, he was with Siemens Electromedical Systems, Danvers, MA. From 1994 to 1999, he was with National Chung-Hsing University, Taichung, Taiwan. Since 1999, he has been a Professor with the Department of Electrical Engineering and the Graduate Institute of Communication Engineering, National Taiwan University. His research interests are electromagnetic applications and system issues, including radio-frequency module and transceiver design, vehicle and satellite navigation, antennas, sensor technology, and wave propagation in the ionosphere.